Ratchetting Behaviour of High Strength Rail Steel under Uniaxial and Biaxial Cyclic Loadings

Chung Lun Pun[1], Qianhua Kan[2], Peter Mutton[3], Guozheng Kang[2], Wenyi Yan[1,*]

[1] Department of Mechanical and Aerospace Engineering, Monash University, Clayton, VIC 3800, Australia
[2] School of Mechanics and Engineering, Southwest Jiaotong University, Chengdu, 610031, People's Republic of China
[3] Institute of Railway Technology, Monash University, Clayton, VIC 3800, Australia
* Corresponding author: wenyi.yan@monash.edu

Abstract   An experimental study was carried out to investigate the cyclic deformation characteristic and ratchetting behaviour of a hypereutectoid high strength rail steel subjected to uniaxial and non-proportionally compression-torsion cyclic loadings. The cyclic deformation characteristic of the material was investigated under uniaxial symmetrical strain cycling. The uniaxial ratchetting was studied under asymmetrical stress cycling with different mean stresses and stress amplitudes and the multiaxial ratchetting was investigated under stress cycling with different axial stresses, equivalent stress amplitudes and non-proportional loading paths. It is shown that the responding stress amplitude decreases with cyclic number, i.e., the steel exhibits cyclic softening under uniaxial symmetrical strain cycling. The uniaxial ratchetting strain increases with mean stress and stress amplitude, but behaves differently under tension and under compression. The multiaxial ratchetting behaviour strongly depends not only on the axial stress and equivalent shear stress amplitudes but also on the non-proportional loading path. Additionally, the material reaches cyclic stabilization after a certain number of loading cycles under both uniaxial and multiaxial stress cyclings. These results can be applied to develop a reliable multiaxial cyclic plasticity model for investigating the degradation behaviour of the high strength rail steel under cumulative wheel-rail contact.

Keywords   Ratchetting, high strength rail steel, non-proportionally multiaxial loading, cyclic loading.

1. Introduction

In the wheel/rail rolling contact process, the rail is subjected to a cyclic loading and the mechanical responses are more complicated than that exhibited under monotonic loading. The rail degradation modes, wear and rolling contact fatigue, are the result of the accumulation of plastic deformation, so called ratchetting, under severe wheel and rail contact cyclic loading. Generally, the response of an elastic-plastic material subjected to cyclic loading can be categorized into four different levels [1]. If the external load is high and above the plastic shakedown limit or ratchetting threshold, e.g., the contact load in a heavy haul line, new plastic deformation will occur and accumulate, i.e., ratchetting, under each cycle of loading. When the ratchetting strain reaches the ductility of the material, the material will failure at the local point [2], which corresponds to the initiation of wear and rolling contact fatigue, e.g., in the form of head checks in the rail head. Therefore, an investigation on plastic ratchetting in the rail head under cyclic loading is of paramount importance in the development of new rail steel and development of rail maintenance strategy in order to mitigate rail degradation.

To quantify the plastic ratchetting in the rail head accurately, a combined isotropic-kinematic hardening model, which reasonably describes the ratchetting behaviour, has to be applied to simulate the rolling contact between the wheel and the rail. Such models included that developed by Armstrong and Frederick [3] and the one modified by Chaboche [4, 5]. The application of these hardening models requires the calibration of some material properties, including basic mechanical parameters and nonlinear coefficients for nonlinear isotropic and kinematic hardening rules, from monotonic and cyclic tests. Examples of calibrating such parameters for ratchetting studies can be found in recent studies by Fedele et al. [6] and Broggiato et al. [7]. To correlate and calibrate the

material data for the ratchetting models, both uniaxial and multiaxial cyclic loading tests should be carried out. These testing methods have been widely applied to investigate the uniaxial and multiaxial ratchetting behaviour of materials, such as stainless steels and ordinary carbon steels, see [8-15]. It was found that different materials exhibit different ratchetting behaviours. Some experimental results of ratchetting behaviour of rail steels under uniaxial and multiaxial strain/stress cycling have also been reported in [16-21]. Four rail steels used in their studies exhibit different features from each other. Therefore, to accurately model the cyclic stress-strain behaviour of a specific material, it is essential to carry out carefully designed uniaxial and multiaxial cyclic loading tests in order to reveal its cyclic deformation characteristics.

In the case of wheel/rail contact, the cyclic compression-torsion test is one of the most appropriate methods to simulate the loading experienced by rail steel in the rail head due to rolling contact between the wheel and the rail. The objective of present study is to experimentally investigate the ratchetting behaviour of a high strength rail steel, which is currently used in heavy haul railways in Australia, under uniaxial and biaxial compression-torsion cyclic loadings at room temperature.

2. Experimental Setup

The material studied herein is a hypereutectoid rail steel with carbon content of 0.85%, which is currently used in heavy haul railways in Australia. Uniaxial cyclic tests were performed on the round solid specimens with test section diameter of 5 mm and length of 30mm, see Fig. 1a. Biaxial compression-torsion tests were performed on thin-walled tubular specimens with outside diameter of 16 mm, inside diameter of 13 mm, and length of 30mm in the test section, see Fig. 1b. All specimens were machined from the rail head of a new flat bottom rail which has the mass of 68 kilogram per metre. The hole in the tubular specimen was made by deep hole drilling operation.
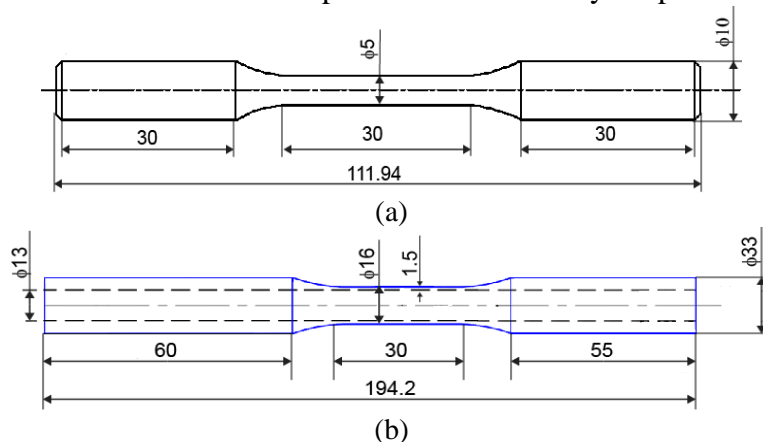
Figure 1. Drawing of (a) round solid specimen for uniaxial cycling tests; (b) thin-walled tubular specimen for biaxial compression-torsion stress cycling tests.

All tests were conducted at room temperature by employing a servo-valve controlled elector-hydraulic testing machine MTS809-250kN, which has the capacity to control axial force and torque independently. The testing process was controlled and the data were collected by a Teststar II control system. A tension-torsion extensometer with 25 mm gauge length and limit of axial strain of ±10% and shear angle of ±5° was employed to measure the axial elongation and torsional angle. Loading rates of strain cycling and stress cyclic were 0.2% s^{-1} and 200MPa s^{-1}, respectively. The total number of loading cycles in each case was 100.

The specimen was first tested under monotonic tensile test in order to obtain some basic mechanical parameters, such as, yield strength and ultimate tensile strength. Following the monotonic tensile test, the deformation behaviour of the specimen under symmetrical strain cycling was observed

from the relationship between the stress amplitude and the number of loading cycle. The maximum and minimum of axial stress σ_{max} and σ_{min} in each cycle was obtained from the collected experimental data and so the stress amplitude σ_a can be determined as,

$$\sigma_a = \frac{1}{2}\left(\sigma_{max} - \sigma_{min}\right) \tag{1}$$

After that, the ratchetting behaviour of the specimen under uniaxial and biaxial compression-torsion stress cycling with different mean stresses and stress amplitudes was studied. Under asymmetrical stress cycling, the maximum and minimum of axial strain ε_{max} and ε_{min} and the maximum and minimum of shear strain γ_{max} and γ_{min} in each cycle were obtained from the collected experimental data. Due to the unclosed hysteresis loop produced under asymmetric stress cycling, the axial ratchetting strain ε_r and torsional ratchetting strain γ_r are defined as:

$$\varepsilon_r = \frac{1}{2}\left(\varepsilon_{max} + \varepsilon_{min}\right) \tag{2}$$

$$\gamma_r = \frac{1}{2}\left(\gamma_{max} + \gamma_{min}\right) \tag{3}$$

Ratchetting strain rates are then defined as $d\varepsilon_r/dN$ and $d\gamma_r/dN$, i.e., the increment of ratchetting strains ε_r and γ_r per cycle. The ratchetting behaviour of the specimen under different loadings can be illustrated by the curve of ratchetting strain versus number of cycles. To investigate the influence of multiaxial loading path on the ratchetting behaviour of the material, five loading paths shown in Fig. 2 were adopted, where σ and $\sqrt{3}\tau$ represent the axial stress and the equivalent shear stress, respectively. In compression-torsion loading paths, the von Mises equivalent stress and strain can be determined as,

$$\sigma_{eq} = \sqrt{\sigma^2 + 3\tau^2} \tag{4}$$

$$\varepsilon_{eq} = \sqrt{\varepsilon^2 + \frac{\gamma^2}{3}} \tag{5}$$

where τ and γ represent the shear stress and shear strain and ε is the axial strain. Therefore, the equivalent shear stress and the equivalent shear strain under pure torsion can be defined as $\sqrt{3}\tau$ and $\gamma/3$, respectively.

(a) Linear A   (b) Oblique   (c) Rectangular

(d) Butterfly   (e) Elliptical
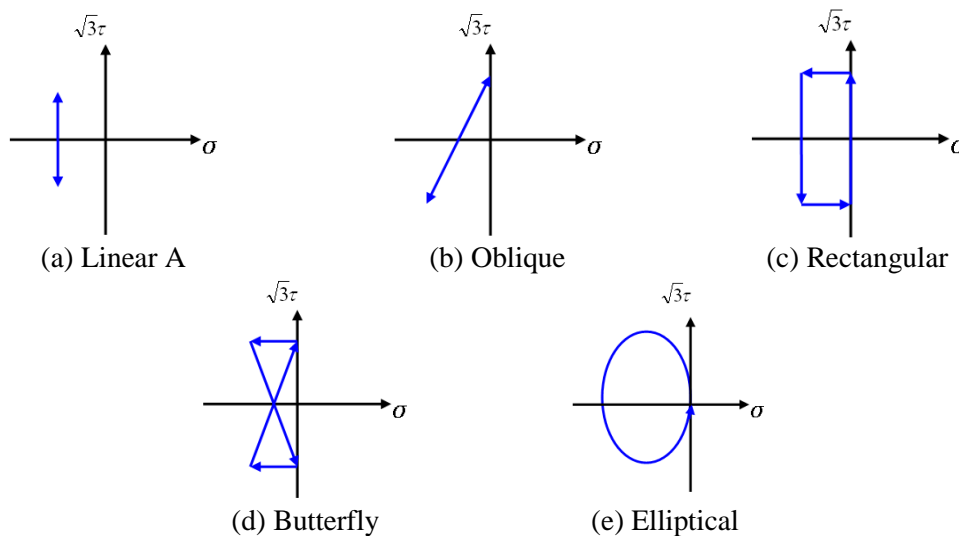
Figure 2. Loading paths for compression-torsion stress cycling.

3. Results

The tensile stress-strain curve for round solid specimen is shown in Fig. 3. The experimental results of elastic modulus E, nominal yield strength $\sigma_{0.2}$, ultimate tensile strength σ_b and elongation δ are 212 GPa, 910 MPa, 1384 MPa and about 12%, respectively.
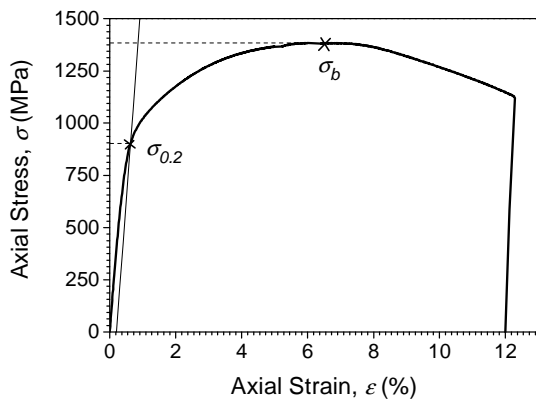
Figure 3. Monotonic tensile stress-strain curve of round solid specimen.
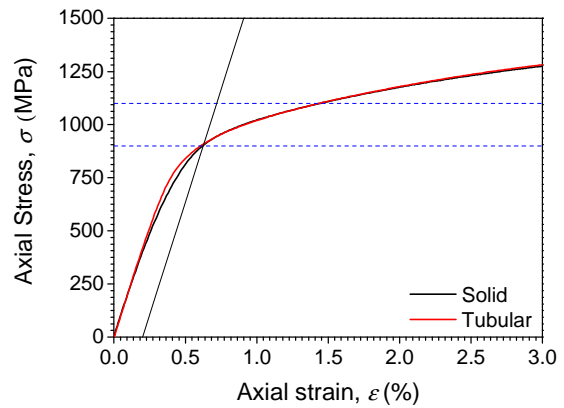
Figure 4. Comparison of mechanical responses from round solid and tubular specimens under monotonic tensile test.

To understand the effect of the specimen design on the measured mechanical properties, a monotonic tensile test was also performed on the tubular specimen. The stress-strain curves from the round solid and the tubular specimens are shown in Fig. 4. The comparison clearly shows that the measured curve of the tubular specimen agrees well with that of the solid specimen in the plastic region and both of them give the same nominal yield strength $\sigma_{0.2}$ of 910 MPa. The discrepancy in the elastic region is negligibly small. Based on the monotonic tensile stress-strain curves of the material, the peak stress applied in the uniaxial stress cycling and the multiaxial stress cycling was selected in the range of 910 MPa to 1100 MPa as illustrated by the dotted horizontal line in Fig. 4.

3.1 Uniaxial strain cycling

The specimen was tested under symmetrical strain cycling at room temperature with the strain amplitude of 0.8%. The cyclic hysteresis loop under uniaxial symmetrical strain cycling is shown in Fig. 5. The results clearly show that the size of the hysteresis loop decreases with the increase of number of cycles. To clearly identify the deformation behaviour of the material under uniaxial strain cycling, the curve of stress amplitude σ_a versus number of cycles N is shown in Fig. 6. It clearly illustrates that the material features cyclic softening remarkably over the first 10 cycles. The decreased rate of stress amplitude in the beginning stage is the largest and reaches a stable value after a certain number of cycles. Similar deformation behaviour was also found in ordinary carbon rail steel and heat-treated rail steel [19]. However, the cyclic softening of the hypereutectoid rail steel in current study is more remarkable.
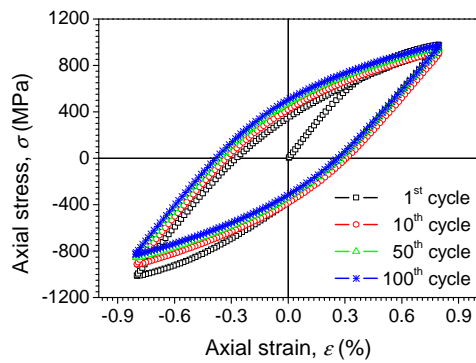
Figure 5. Cyclic hysteresis loops under uniaxial symmetrical strain cycling with strain amplitude of 0.8%.
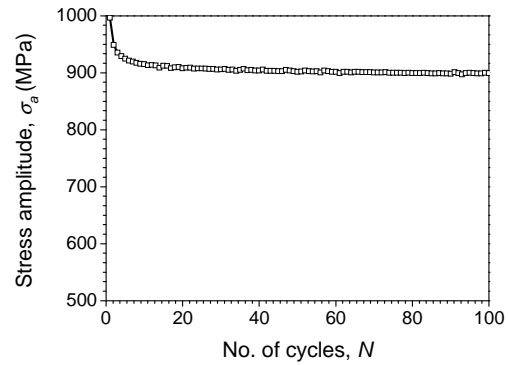
Figure 6. Diagram of stress amplitude σ_a versus number of loading cycle N under uniaxial symmetrical strain cycling with strain amplitude of 0.8%.

3.2 Uniaxial stress cycling

To observe the ratchetting behaviour of hypereutectoid rail steel under uniaxial asymmetrical stress cycling at room temperature, the material was tested with different mean stresses and stress amplitudes. Fig. 7a demonstrates the cyclic hysteresis loops of the specimen under an asymmetrical stress cycling with load condition of 200 ± 800 MPa. The results clearly show that ratchetting occurs under the asymmetrical stress cycling. The hysteresis loop becomes smaller and smaller at the beginning of cycling. After certain cycles, it almost keeps unchanged in the remaining cycles. Similar ratchetting behaviour can be found in the asymmetrical stress cycling with load condition of 200 ± 900 MPa and 100 ± 900 MPa as shown in Fig. 7b and 7c, respectively.
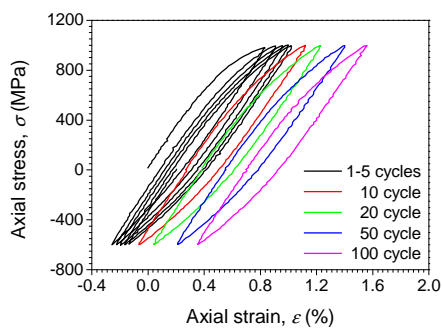
(a)
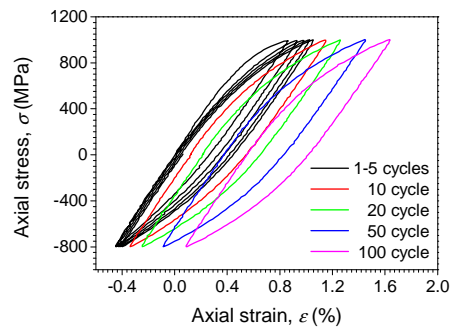
(b)
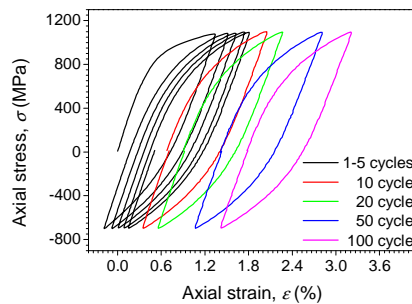
(c)

Figure 7. Cyclic hysteresis loops under asymmetrical stress cycling with load condition of (a) 200 ± 800 MPa; (b) 200 ± 900 MPa; (c) 100 ± 900 MPa.

To clearly illustrate the influence of stress amplitude on the ratchetting behaviour of the material, the axial ratchetting strain, which is determined by following Eq. (2), and the ratchetting strain rate versus number of cycles with different stress amplitudes are shown in Figs. 8a and 8b, respectively. The results clearly demonstrate that both ratchetting strain and ratchetting strain rate increase with stress amplitude. Furthermore, the axial ratchetting strain increases but the ratchetting strain rate decreases continuously with the increasing number of loading cycles. After about 10 cycles for $\sigma_a = 800$ MPa and about 15 cycles for $\sigma_a = 900$ MPa, the ratchetting strain rate becomes very small and almost remains constant over the remaining cycles.

(a)   (b)
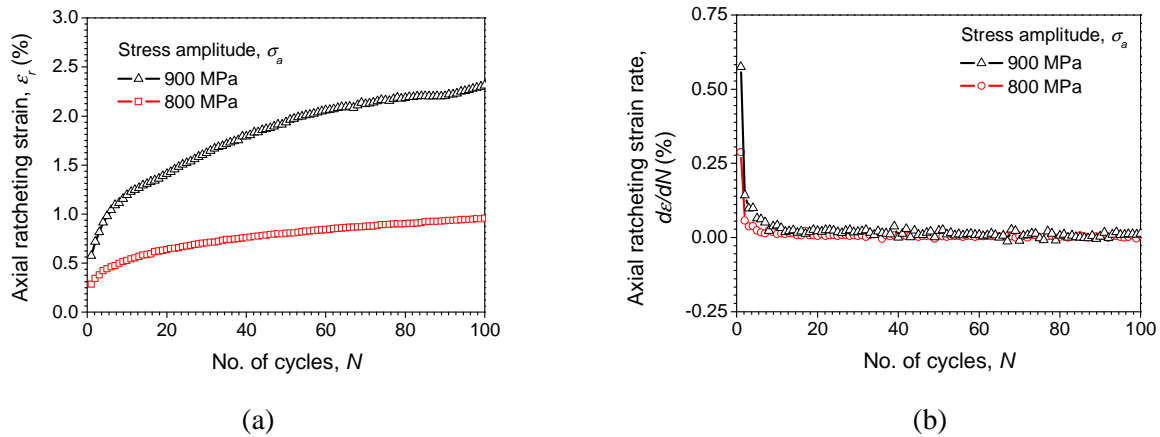
Figure 8. (a) Axial ratchetting strain ε_r; (b) Axial ratchetting strain rate $d\varepsilon_r/dN$, versus number of cycles N with different stress amplitude σ_a while the mean stress σ_m is kept constant in all cases.

(a)   (b)
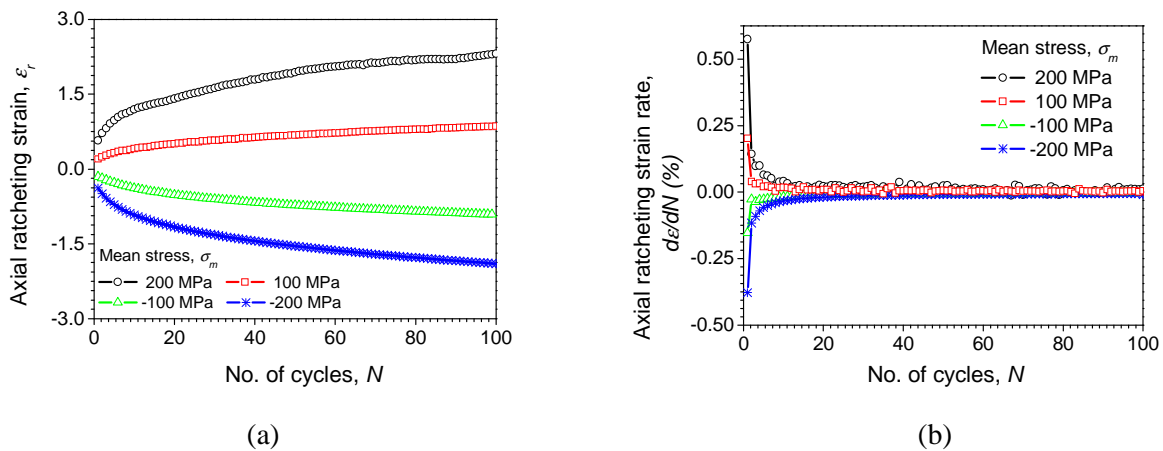
Figure 9. (a) Axial ratchetting strain ε_r; (b) Axial ratchetting strain rate $d\varepsilon_r/dN$, versus number of cycles N with different mean stress σ_m while the stress amplitude σ_a is kept constant in all cases.

Figs. 9a and 9b show the ratchetting strain ε_r and the ratchetting strain rate $d\varepsilon_r/dN$ versus number of cycles N with different mean stresses. The results show that both ratchetting strain and ratchetting strain rate increase with the mean stress. After certain cycles, the ratchetting strain rate $d\varepsilon_r/dN$ becomes very small and remains constant over the remaining cycles. It is also found that the material requires more cycle to stabilize when the mean stress is higher. Additionally, the results indicate that negative mean stress does not provide a perfectly symmetrical result as the positive mean stress does. This means that the material has a slight difference in ratchetting behaviour under tension and under compression. Furthermore, both Figs 8b and 9b show that the axial ratchetting strain rate decreases with increasing number of loading cycles and becomes almost constant in the remaining cycles, which indicates that the ratchetting of the material is dominated by kinematic

hardening and so a cyclic stabilization is reached after certain number of cycles under uniaxial stress cycling.

3.3 Compression-torsion stress cycling

Under the loading paths shown in Figs 3a to 3e, the material was tested under compressive-torsional stress cycling with different mean stresses and stress amplitudes. The relation between ratchetting behaviour and non-proportionally multiaxial loading path is also discussed. Experimental results of two of the loading cases are shown in Fig 10a and 10b. The case shown in Fig. 11a is under symmetrical torsional stress cycling and the results clearly show that the axial ratchetting is the dominant while the torsional ratchetting is relatively small and can be neglected. The same evolution tendency of ratchetting strain can be found in the stress cycling under elliptical path as illustrated in Fig 11b, and the other three paths. Comparing Fig. 10a and 10b, it is found that the absolute value of ratcheting strain at 100 cycles for elliptical path is smaller than that for linear path (1.5% to 3.0%).

| (a) | (b) |
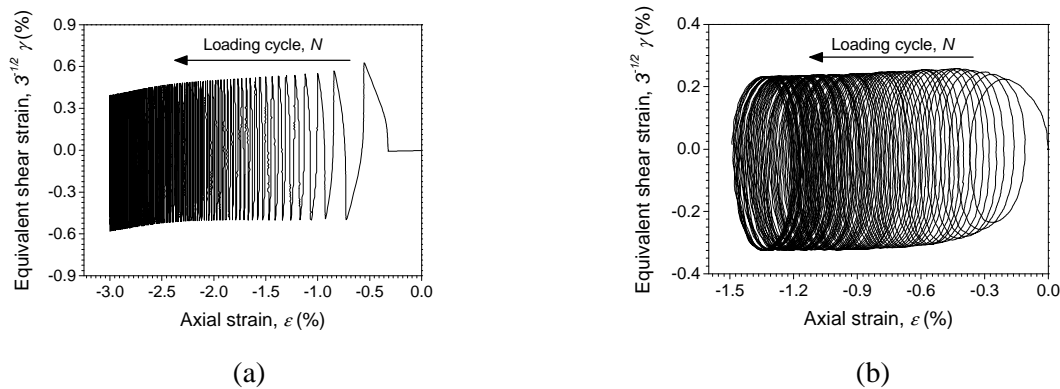
Figure 10. Experimental results of equivalent shear strain $\gamma/\sqrt{3}$ versus axial strain, ε under (a) linear path; and (b) elliptical path with the same loading condition of $\sigma_{eq} = 1019.8$ MPa.

Figs. 11a and 11b demonstrate the influence of axial stresses on the ratchetting behaviour under linear path while the equivalent shear stress $\sqrt{3}\tau$ is kept constant as 0 ± 1000 MPa for all cases. The results show that ratchetting takes place when axial stress σ is high enough. Both axial ratchetting strain ε_r and axial ratchetting strain rate $d\varepsilon_r/dN$ increases with axial stress σ. Additionally, the ratchetting behaviour of the material depends on the equivalent shear stress amplitude under linear path, as shown in Figs. 12a and 12b. For all the cases, the axial stress σ and the mean equivalent shear stress $\left(\sqrt{3}\tau\right)_m$ are kept constant as -200 MPa and 0 MPa, respectively. The results indicate that both axial ratchetting strain ε_r and axial ratchetting strain rate $d\varepsilon_r/dN$ increases with the equivalent shear stress amplitude $\left(\sqrt{3}\tau\right)_a$.

The ratchetting behaviour of the specimen is significantly influenced not only by the axial stress and the equivalent shear stress amplitude but also by the non-proportional loading path as illustrated in Figs. 13a and 13b. For all cases, the applied equivalent stress σ_{eq} is kept constant as 1019.8 MPa. The results show that the non-proportional loading path influences not only the axial ratchetting strain ε_r but also the axial ratchetting strain rate $d\varepsilon_r/dN$. Among all the five loading paths, the elliptical path gives the lowest ratchetting strain and rate. When N is less than 65, the linear path gives the highest ratchetting strain. When N is larger than 65, the highest ratchetting strain is contributed by the rectangular path.

(a)

(b)
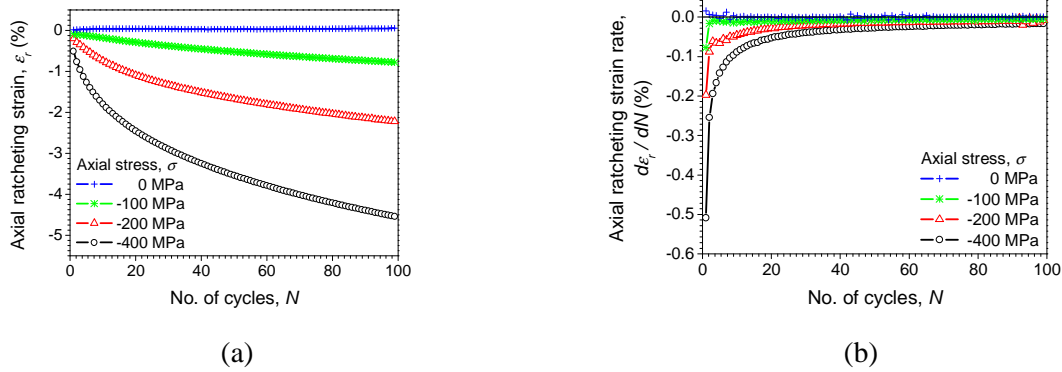
Figure 11. (a) Axial ratchetting strain ε_r; (b) Axial ratchetting strain rate $d\varepsilon_r/dN$, versus number of cycles N under linear path with different axial stress σ while the equivalent shear stress $\sqrt{3}\tau$ is kept constant.

(a)

(b)
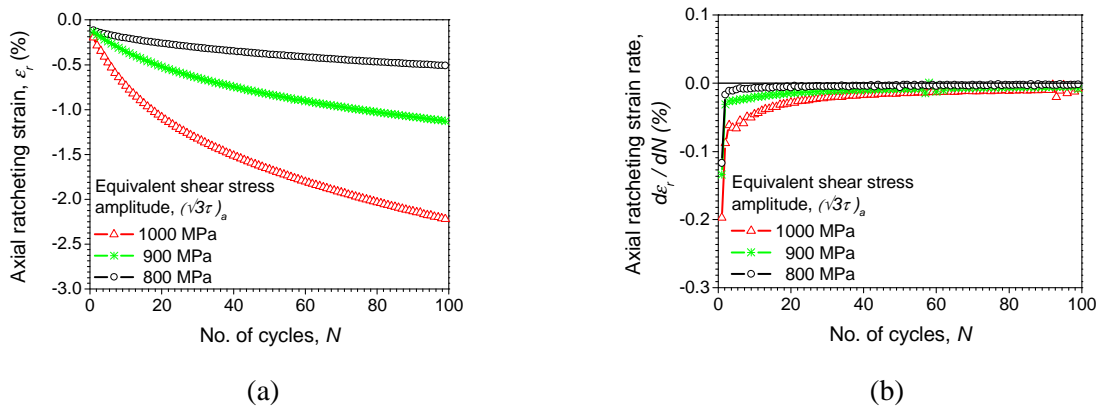
Figure 12. (a) Axial ratchetting strain ε_r; (b) Axial ratchetting strain rate $d\varepsilon_r/dN$, versus number of cycles N under linear path with different equivalent shear stress amplitude $\left(\sqrt{3}\tau\right)_a$ while the axial stress is kept constant.

(a)

(b)
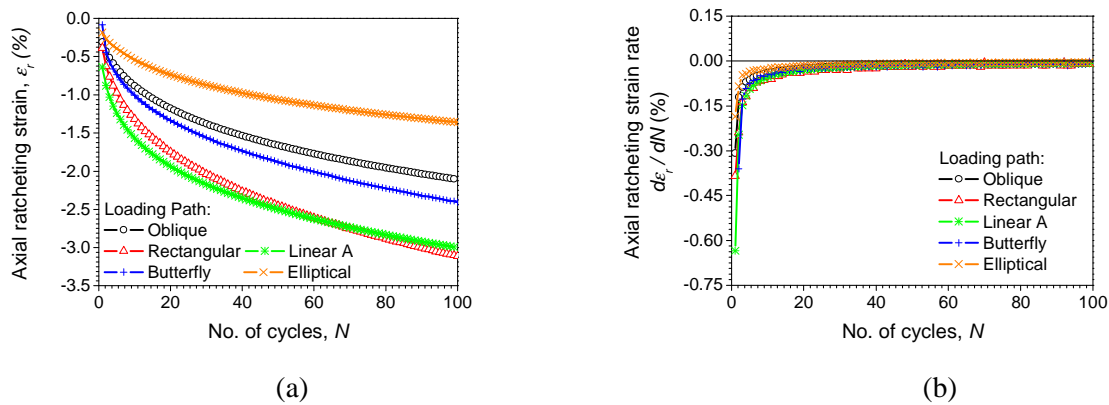
Figure 13. (a) Axial ratchetting strain ε_r; (b) Axial ratchetting strain rate $d\varepsilon_r/dN$, versus number of cycles N with different non-proportional loading paths while the applied equivalent stress σ_{eq} is kept constant.

It is worth noting that Figs 11, 12 and 13 demonstrate that the axial ratchetting strain increases but its rate decreases continuously with increasing number of cycles. After a certain number of cycles, the axial ratchetting strain rate becomes very small and almost remains constant in the remaining cycles. Therefore, it can be concluded that the ratchetting of the material under multiaxial stress cycling is dominated by kinematic hardening and so a cyclic stabilization is reached after certain number of cycles, i.e. about 45 cycles when $\sigma = -200$ MPa in Fig 12b. It is also found that the increase of axial stress and equivalent shear stress lead to increase the required cyclic number to

reach cyclic stabilization of the material. Moreover, it is indicated from Fig 13a that the nonproportional additional hardening will restrain the ratchetting strain even under compression-torsion loading, which is consistent with [14] under tension-torsion loading. The elliptical path is more relevant to actual wheel/rail contact situations as the contact patch was often found to be elliptical in shape which implies that the relative weak ratchetting behaviour will occur in real wheel/rail rolling contact process. These features and their effects on ratchetting should be taken into account in cyclic constitutive model development in the future.

4. Conclusion

A hypereutectoid grade high strength rail steel, which is currently used in heavy haul operation in Australia, has been tested under uniaxial and compression-torsion cyclic loadings. The elastic modulus, nominal yield strength and ultimate tensile strength of the material are found as 212 GPa, 910 MPa and 1384 MPa, respectively. Under symmetrical strain cycling, the material exhibits cyclic softening at the start and then stabilizes quickly. Although this material's behaviour is similar to those found in the literature, the cyclic softening of the hypereutectoid rail steel is more remarkable.

Under uniaxial stress cycling, ratchetting behaviour strongly depends on mean stress and stress amplitude. Both ratchetting strain and ratchetting rate increase with mean stress and stress amplitude. The material stabilizes after certain number of loading cycles and the required number of cycles to reach cyclic stabilization also depends on mean stress and stress amplitude. It is found that the ratchetting of the material behaves slightly different under tension and compression.

Under multiaxial stress cycling, ratchetting is significantly influenced by axial stress, equivalent shear stress amplitude and non-proportional loading path. Both ratchetting and ratchetting strain rate increases with axial stress and equivalent shear stress amplitude. It is also found that kinematic hardening is dominant in the ratchetting of the material. It reaches cyclic stabilization after certain number of loading cycles and the required cyclic number is also influenced by the axial stress and equivalent shear stress amplitude. Among all the five studied loading paths, the elliptical loading path is more relevant to actual wheel/rail contact situations and it gives the lowest ratchetting strain and ratchetting strain rate.

References
[1] A. Kapoor, K.L. Johnson, Plastic ratchetting as a mechanism of metallic wear. Proc R Soc Lond, A445 (1994) 367-384.
[2] A. Kapoor, A re-evaluation of the life to rupture of ductile metals by cyclic plastic strain. Fatigue Fract Engng Mater Struct 17 (1994) 201-219.
[3] P.J. Armstrong, C.O. Frederick, A mathematical representation of the multiaxial Bauschinger effect, CEGB Report RD/B/N731, Berkely Nuclear Laboratories, Berkely, UK, 1966.
[4] J.L. Chaboche, Time-independent constitutive theories for cyclic plasticity. Int J Plast 2 (1986) 149-188.
[5] J.L. Chaboche, Constitutive equations for cyclic plasticity and cyclic viscoplasticity. Int J Plast 5 (1989) 247-302.
[6] R. Fedele, M. Filippini, G. Maier, Constitutive model calibration for railway wheel steel through tension-torsion tests. Comput and Struct 83 (2005) 1005-1020.

[7]   G.B. Broggiato, F. Campana, L. Cortese, The Chaboche nonlinear kinematic hardening model: calibration methodology and validation. Meccanica 43 (2008) 115-124.

[8]   F. Yoshida, Uniaxial and biaxial creep-ratchetting behaviour of SUS304 stainless steel at room temperature. Int J Press Ves Pip 44 (1990) 207-223.

[9]   T. Hassan, S. Kytriakides, Ratcheting in cyclically hardening and softening materials: I. Uniaxial behavior. Int J Plast 10(2) (1994) 149-184.

[10] T. Hassan, S. Kyriakides, Ratcheting in cyclically hardening and softening materials: II. Multiaxial behaviour. Int J Plast 10(2) (1994) 185-212.

[11] P. Delobelle, P. Robinet, L. Bocher, Experimental study and phenomenological modelization of ratchet under uniaxial and biaxial loading on an austenitic stainless steel. Int J Plast 11(4) (1995) 295-330.

[12] M. Mizuno, Y. Mima, M. Abdel-Karim, N. Ohno, Uniaxial ratchetting of 316FR steel at room temperature-- Part 1: Experiments. ASME J Eng Mater Technol 122(1) (2000) 29-34.

[13] G.Z. Kang, Q. Gao, X.J. Yang, Y.F. Sun, An experimental study on uniaxial and multiaxial strain cyclic characteristics and ratcheting of 316L stainless steel. J Mater Sci Technol 17(1) (2001) 219-223.

[14] G.Z. Kang, Q. Gao, X.J. Yang, Uniaxial and non-proportionally multiaxial ratcheting of SS304 stainless steel at room temperature: experiments and simulations. Int J Nonlinear Mech 39 (2004) 843-857.

[15] G.Z. Kang, Y.G. Li, J. Zhang, Y.F. Sun, Q. Gao, Uniaxial ratcheting and failure behaviors of two steels. Theor Appl Fract Mech 43 (2005) 199-209.

[16] A.F. Bower, Cyclic hardening properties of hard-drawn copper and rail steel. J Mech Phys Solids 37(4) 455-470.

[17] D.L. McDowell, On the path dependence of transient hardening and softening to stable states under complex biaxial cyclic loading. In: Desai, C.S., Gallagher, R.H. (Eds), Proceeding of International Conference on Constitutive Laws for Engineering Materials: Theory and Application, Univ Arizona, Tucson, AZ, 1983, pp. 125-131.

[18] D.L. McDowell, An evaluation of recent developments in hardening and flow rules for rate independent nonproportional cyclic plasticity. ASME J Appl Mech 54 (1987) 323-331.

[19] D.L. McDowell, Stress state dependence of cyclic ratchetting behaviour of two rail steels. Int J Plast 11(4) (1995) 397-421.

[20] G.Z. Kang, Q. Gao, X.J. Yang, Experimental study on the cyclic deformation and plastic flow of U71Mn rail steel. Int J Mech Sci 44 (2002) 1647-1663.

[21] G.Z. Kang, Q. Gao, Uniaxial and non-proportionally multiaxial ratcheting of U71Mn rail steel: experiments and simulations. Mech Mater 34 (2002) 809-820.